JOURNAL OF SPACECRAFT AND ROCKETS
Vol. 33, No. 2, March–April 1996

Electric-Propulsion Spacecraft Optimization for Lunar Missions

Craig A. Kluever* and Kun-Rong Chang†
University of Missouri—Columbia/Kansas City, Kansas City, Missouri 64110-2499

A quick and efficient method for computing the optimal vehicle–trajectory combination for lunar missions using electric propulsion is developed. The problem involves computing the optimal spacecraft sizing parameters and trajectory shaping parameters that maximize the payload for a one-way, fixed-trip-time, planar transfer from circular Earth orbit to circular low lunar orbit. The computational load of the problem is reduced by utilizing universal low-thrust trajectory solutions to approximate the Earth-escape and moon-capture spiral trajectories. Several maximum-payload solutions are obtained for both nuclear electric-propulsion and solar electric-propulsion spacecraft. The nuclear results show a very good match with published exact trajectories. A sensitivity analysis of the assumed electric-propulsion technology level is also performed.

Nomenclature

a_T	= thrust acceleration, m/s^2
b	= propellant-dependent coefficient
c	= engine exhaust velocity, km/s
D	= constant Earth–moon separation distance, km
d	= propellant-dependent coefficient, km/s
g	= sea-level gravitational acceleration, m/s^2
I_{sp}	= specific impulse, s
K_t	= tankage fraction
m_{net}	= net mass of spacecraft, kg
m_{pp}	= mass of power and propulsion system, kg
m_{prop}	= propellant mass, kg
m_{tank}	= mass of tank and propellant feed system, kg
m_0	= initial mass of spacecraft in Earth orbit, kg
P	= input power, kW
r	= radial position, km
T/W	= thrust-to-weight ratio
t_{capt}	= powered moon-capture spiral time, days
t_{coast}	= translunar coast time, days
t_{esc}	= powered Earth-escape spiral time, days
t_f	= total trip time, days
v_r	= radial velocity, km/s
v_θ	= circumferential velocity, km/s
α	= power and propulsion system specific mass, kg/kW
η	= thruster efficiency
θ	= polar angle, deg
μ	= gravitational parameter
μ_{net}	= net mass fraction
ω	= constant Earth–moon system angular rate, rad/s

Subscripts

e	= Earth
m	= moon
LEO	= low Earth orbit
LLO	= low lunar orbit

Superscript

$*$	= nominal or optimal value

Introduction

IT has been established that electric-propulsion (EP) spacecraft can deliver a greater payload fraction for a given space mission than chemical-propulsion spacecraft. The tradeoff for the enhanced payload capability is an increase in total transfer time. A particular mission of interest involves the low-thrust transfer from circular Earth orbit to circular lunar orbit.[1–3] References 1–3 present solutions to an EP vehicle-trajectory optimization problem for lunar missions, and a variety of trajectory analysis methods are utilized to compute the long-duration, low-thrust spiral trajectories about the Earth and moon. In Ref. 1, Gilland obtained optimal vehicle–trajectory solutions for nuclear electric-propulsion (NEP) spacecraft for both lunar and Mars cargo missions by utilizing a simple analytic expression to approximate the velocity increment required for the orbit transfer. Palaszewski[2] has investigated EP vehicle sizing for lunar missions using both NEP and solar electric propulsion (SEP) with ion, arcjet, and magnetoplasmadynamic thrusters, and the corresponding orbit transfer analysis was similar to the method of Ref. 1. Both trajectory analysis methods from Refs. 1 and 2 assume that the lunar mission consists of a continuous-thrust orbit transfer without coasting arcs. In Ref. 3, optimal vehicle–trajectory solutions for NEP lunar missions are obtained by using trajectory optimization methods coupled with a detailed simulation of the governing equations of motion. The transfer orbit is computed through numerical integration, and a single translunar coast arc is included. Although the results are highly accurate, the procedure is numerically intense.

In this paper, we demonstrate a quick and efficient method for computing the optimal EP vehicle sizing parameters and trajectory shaping parameters for a one-way, planar transfer from circular Earth orbit to circular low lunar orbit (LLO). The optimization problem involves maximizing the payload fraction for a fixed transfer time, and the free vehicle parameters are the specific impulse I_{sp} and electric input power P. The lunar transfer is assumed to consist of a powered Earth-escape spiral, followed by a translunar coast, and finally a powered moon-capture spiral to LLO. The trajectory design parameters are the initial Earth–moon geometry and the durations of the two powered phases. Numerical results are presented for a wide range of trip times for both NEP and SEP spacecraft, and a sensitivity analysis of the assumed technology level is performed.

Maximum-Payload Problem

Spacecraft System Analysis

The objective of the vehicle-trajectory optimization problem is to maximize the net mass of the spacecraft for a fixed-time transfer from a prescribed circular Earth orbit to LLO. The net mass m_{net} is defined as

$$m_{net} = m_0 - m_{prop} - m_{tank} - m_{pp} \tag{1}$$

The spacecraft's net mass represents the usable mass for payload plus the basic spacecraft structural mass. For preliminary analyses, the structural mass can be computed[4] as a percentage (5–10%) of the initial mass m_0. The tank mass m_{tank} is the product of the tankage fraction K_t and the total propellant mass m_{prop}. The mass of the

Received June 13, 1995; revision received Oct. 13, 1995; accepted for publication Nov. 13, 1995.

*Assistant Professor, Mechanical and Aerospace Engineering Department. Member AIAA.

†Graduate Research Assistant, Mechanical and Aerospace Engineering Department.

Table 1 Vehicle parameters and boundary conditions

Case	Propulsion mode	α, kg/kW	K_t	Initial Earth alt., km	Lunar alt., km	m_0, kg
1	NEP	7.3	0.05	407	100	123,000
2	NEP	25	0.15	407	100	123,000
3	SEP	25	0.10	35,786	100	2,140

power and propulsion system, m_{pp}, is the product of the specific mass α and input power P. The vehicle parameters K_t and α represent the assumed technology level for the NEP and SEP spacecraft, and their values along with m_0 and the boundary orbits for the lunar missions are presented in Table 1. Case 1 in Table 1 corresponds to the lunar mission and fixed vehicle parameters from Ref. 3 and represents a projected technology level for an NEP lunar cargo spacecraft in the 2010 time frame. Although the vehicle parameters for case 1 are fairly optimistic, the objective here is to make a direct comparison with the results from Ref. 3. Case 2 represents current or near-term technology for an NEP lunar cargo spacecraft with vehicle parameters from Refs. 1 and 5. The mission boundary conditions for case 2 are the same as for case 1. Case 3 represents an SEP vehicle envisioned for scientific exploration of the moon. The SEP vehicle parameters are from Refs. 6–7 and represent the current technology level. The initial mass m_0 corresponds to the launch capability to geosynchronous orbit (GEO) of the Atlas IIAS. Selecting GEO as the initial orbit for the SEP probe nearly eliminates Earth-shadowing (and therefore unpowered) conditions and also alleviates solar-cell degradation from the Van Allen radiation belts.

It is assumed that xenon is utilized as the propellant for both the NEP and SEP vehicles. The thruster efficiency η is determined by the relation below, using I_{sp} and propellant-dependent coefficients derived from theoretical models and experimental data[1]:

$$\eta = \frac{bc^2}{c^2 + d^2} \tag{2}$$

where the exhaust velocity $c = I_{sp} g$ and where $b = 0.81$ and $d = 13.5$ km/s. The specific impulse is bounded between 3000 and 7000 s for the NEP spacecraft (cases 1 and 2), and between 2000 and 7000 s for the SEP spacecraft (case 3).

The total propellant mass is the product of the propellant mass flow rate $\dot{m}$ and the total engine-on time. The total engine-on time is the sum of the powered Earth-escape spiral time t_{esc} and the powered moon-capture spiral time t_{capt}. The mass flow rate is a function of efficiency η, power P, and I_{sp}:

$$\dot{m} = (2\eta P)/c^2 \tag{3}$$

The vehicle parameters P and I_{sp} are considered to be fixed over the duration of the lunar transfer, which is equivalent to a fixed operating point and no engine throttling.

Trajectory Analysis

The planar Earth–moon transfer with a fixed thrust–coast–thrust engine sequence is approximated by patching together the two powered escape–capture spiral trajectories with the numerically integrated coasting trajectory. The intense computational load of the trajectory optimization method in Ref. 3 is a result of the numerical integration of the long-duration, many-revolution escape and capture spirals about the Earth and moon. For our trajectory analysis method here, we replace the escape and capture spirals with curve fits of universal low-thrust spiral-trajectory solutions. Perkins[8] developed a set of planar differential equations independent of initial circular radius, thrust acceleration, or attracting body that approximate the motion of a low-thrust spacecraft in an inverse-square gravity field with a constant thrust acceleration vector pointed along the instantaneous velocity vector. Three nondimensional parametric curves of radial distance, velocity magnitude, and flight-path angle vs transfer time are constructed upon numerical integration of the approximate[8] two-body equations of motion. These universal low-thrust solutions can be scaled by specifying the initial circular orbit radius, the gravitational parameter of the attracting body, and the constant thrust acceleration of the spacecraft. Therefore, the vehicle's state at the end of the powered Earth-escape spiral trajectory (or start of the moon-capture spiral) is obtained by curve-fitting the universal low-thrust solutions with escape time t_{esc} (or capture time t_{capt}) as the independent variable. Next, the nondimensional states are scaled by using the appropriate initial circular radius, gravitational parameter, and thrust acceleration. A functional representation of the boundary conditions at the terminal ends of the coasting trajectory is as follows:

$$r(0) = g_1(r_{LEO}, \mu_e, a_T; t_{esc}) \tag{4}$$

$$v_r(0) = g_2(r_{LEO}, \mu_e, a_T; t_{esc}) \tag{5}$$

$$v_\theta(0) = g_3(r_{LEO}, \mu_e, a_T; t_{esc}) \tag{6}$$

$$r(t_{coast}) = h_1(r_{LLO}, \mu_m, a_T; t_{capt}) \tag{7}$$

$$v_r(t_{coast}) = h_2(r_{LLO}, \mu_m, a_T; t_{capt}) \tag{8}$$

$$v_\theta(t_{coast}) = h_3(r_{LLO}, \mu_m, a_T; t_{capt}) \tag{9}$$

The initial and terminal states for the translunar coasting trajectory are provided by the functional relationships g_1–g_3 and h_1–h_3, which represent numerical curve fits of universal low-thrust spiral-trajectory solutions. The states of the system are the radial position r, radial velocity v_r, circumferential velocity v_θ, and polar angle θ. The gravitational parameters for the Earth and moon are denoted by μ_e and μ_m, respectively. This curve-fitting procedure eliminates the need to numerically integrate the long-duration Earth-escape and moon-capture spirals, and the approximation allows the simple computation of escape and capture spirals for a wide range of P and I_{sp}. Perkins has demonstrated that the universal low-thrust trajectory solutions nearly match exact numerically integrated trajectories for thrust-to-weight (T/W) ratios below 10^{-2}, and that as T/W decreases, the universal solutions become more accurate.

The complete Earth–moon transfer is computed by utilizing the escape–capture curve-fit solutions as boundary conditions and numerically integrating the translunar coasting arc. The dynamics of the coasting arc are governed by the classical restricted three-body problem[9] as follows:

$$\dot{r} = v_r \tag{10}$$

$$\dot{v}_r = \frac{v_\theta^2}{r} - \frac{\mu_e}{r^2} - \frac{\mu_m(r + D\cos\theta)}{(r^2 + 2Dr\cos\theta + D^2)^{\frac{3}{2}}} + \frac{\mu_m \cos\theta}{D^2} + 2\omega v_\theta + \omega^2 r \tag{11}$$

$$\dot{v}_\theta = \frac{\mu_m D\sin\theta}{(r^2 + 2Dr\cos\theta + D^2)^{\frac{3}{2}}} - \frac{\mu_m \sin\theta}{D^2} - 2\omega v_r - \frac{v_r v_\theta}{r} \tag{12}$$

$$\dot{\theta} = v_\theta / r \tag{13}$$

Equations (10–13) are the three-body equations of motion for a coasting spacecraft in a rotating, Earth-centered polar coordinate frame. The x axis is along the Earth–moon line and is considered positive from the Earth center away from the moon. The polar angle θ is measured positive counterclockwise from the x axis.

The terminal states at the end of the integrated coasting arc must match the curve-fit states h_1–h_3 for the moon-capture spiral. Therefore, the Earth–moon trajectory shaping variables are the escape time t_{esc}, capture time t_{capt}, coast time t_{coast}, and initial polar angle $\theta(0)$ at the start of the translunar coast. Low-thrust Earth–moon transfers have been computed using this method for a range of T/W, and the results exhibit a good match with the corresponding numerically integrated Earth–moon trajectories.[10]

Vehicle-Trajectory Optimization

The problem statement for our fixed-end-time vehicle–trajectory optimization problem is as follows: Find the four trajectory shaping parameters t_{esc}, t_{coast}, t_{capt} and $\theta(0)$ and the two vehicle parameters P and I_{sp} that minimize

$$J = -m_{net} \tag{14}$$

subject to the unpowered three-body equations of motion (10–13) with initial state conditions (4–6) and terminal conditions (7–9) and the following constraint for the fixed total trip time:

$$t_f = t_{esc} + t_{coast} + t_{capt} \tag{15}$$

Since most optimization software is designed to minimize a performance index, the maximum payload is obtained by minimizing $-m_{net}$. The maximum-payload problem is solved by using sequential quadratic programming (SQP), a direct parameter optimization method.[11] The SQP code used here computes the gradients with first-order forward differences.[12] The optimization problem involves only six SQP design variables and four equality constraints. Three equality constraints are required to enforce the state-variable matching between the numerically integrated coasting arc and the curve-fit moon-capture states as indicated by Eqs. (7–9). A fourth equality constraint is required to enforce the desired fixed trip time as indicated by Eq. (15). Numerical integration of the coasting trajectory is performed by a standard fourth-order, fixed-step Runge–Kutta routine with 500 integration steps.

Results

Several optimal vehicle and trajectory combinations have been obtained for a wide range of fixed trip times for the three cases outlined in Table 1. The solution method proved to be very robust and efficient, since only six SQP design variables are required and the trajectory approximation curve-fitting scheme eliminates the need to numerically integrate the long-duration spiral trajectories. The optimal net mass fraction $\mu_{net} = m_{net}/m_0$ is presented in Fig. 1 for all three cases. Each point represents an optimal vehicle–trajectory combination for the desired fixed one-way trip time t_f, fixed initial mass m_0, and fixed technology parameters α and K_t. All maximum-payload curves exhibit a steep rise in performance from their respective zero-m_{net} trip times until the trip time is increased and the payload performance levels off. For the projected NEP technology level (case 1), μ_{net} levels off to about 0.77 after 200 days, which corresponds with the results from Ref. 3. Similarly, the near-term NEP (case 2) vehicle's performance levels off in about 280 days to $\mu_{net} = 0.60$, and μ_{net} for the SEP vehicle approaches an asymptotic value of 0.80 after about 200 days.

The corresponding optimal P and I_{sp} values for the respective cases are presented in Figs. 2 and 3. Figure 2 demonstrates how optimal power decreases with increasing trip time. The NEP spacecraft shows a power range from approximately 123,000 to 980 kW. The extremely high optimal NEP power levels correspond to case 1 with relatively short trip times from 20 to 60 days. For the more realistic NEP spacecraft (case 2), the optimal power range is from 3600 to 980 kW, which is consistent with projected NEP power levels.[5] The SEP spacecraft exhibits a power range from approximately 72 to 9 kW, which correspond to the shortest and longest trip times, respectively. Figure 3 shows how the optimal I_{sp} increases at a nearly linear rate with increasing trip time. Furthermore, the optimal I_{sp} reaches the lower operating boundary as the trip is decreased. The optimal payload, power, and I_{sp} curves for case 1 correspond very nicely with the respective curves presented in Ref. 3.

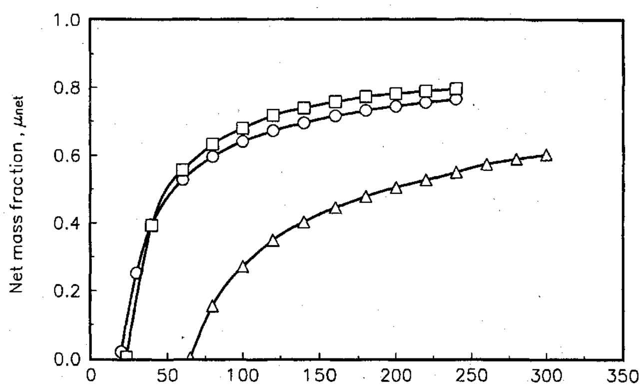

Fig. 1 Optimal net mass fraction vs trip time: ○, case 1; △, case 2; and □, case 3.

Table 2 Optimal vehicle-trajectory solutions vs optimal solutions from Ref. 3

Trajectory analysis	t_f, days	P, kW	I_{sp}, s	t_{esc}, days	t_{coast}, days	t_{capt}, days	μ_{net}
Approx.	65	3956.5	3357.3	49.22	6.96	8.82	0.548
Exact	65	3858.1	3435.6	51.93	3.21	9.86	0.555
Approx.	90	3234.7	4054.6	71.33	4.64	14.04	0.621
Exact	90	3200.4	4032.3	71.41	5.74	12.84	0.625
Approx.	150	2445.2	5274.9	119.92	5.39	24.70	0.707
Exact	150	2396.9	5245.3	121.19	6.58	22.23	0.713
Approx.	200	2114.2	6119.2	160.15	6.12	33.73	0.745
Exact	200	2040.1	6023.6	161.55	7.06	31.39	0.750

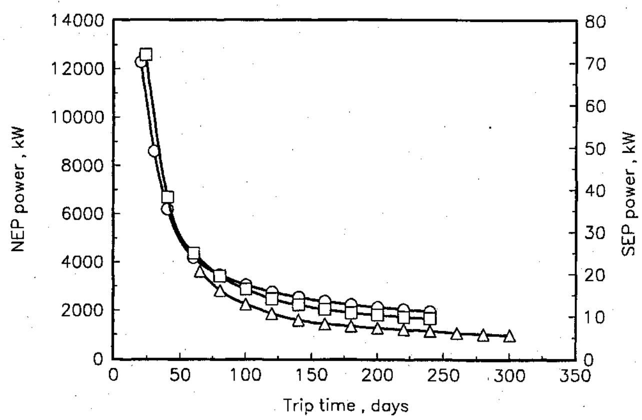

Fig. 2 Optimal power vs trip time: ○, case 1 (NEP); △, case 2 (NEP); and □, case 3 (SEP).

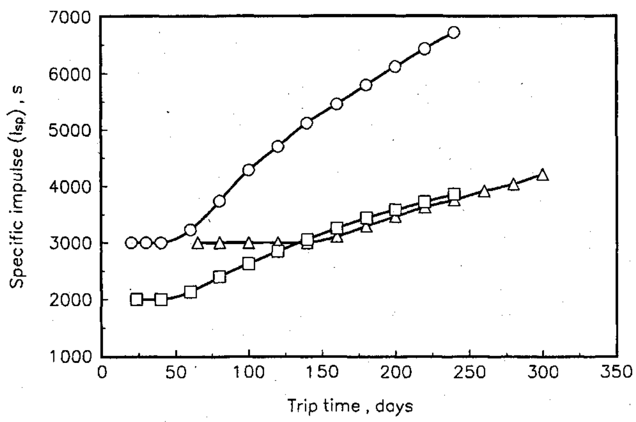

Fig. 3 Optimal I_{sp} vs trip time: ○, case 1; △, case 2; and □, case 3.

As a further demonstration of the accuracy of our quick vehicle–trajectory optimization method, a comparison with the results from Ref. 3 is summarized in Table 2. Recall that in Ref. 3 the trajectory analysis and optimization were performed by utilizing numerical integration of both the powered and coasting trajectories, with the thrust steering computed via optimal-control theory. Our trajectory approximation approach utilizes curve fits of universal low-thrust spiral-trajectory solutions with thrust steering along the velocity vector. Table 2 shows that the optimal vehicle parameters P and I_{sp} and the trajectory segment durations from our trajectory approximation method compare very nicely with the exact trajectory results from Ref. 3. Furthermore, the error in optimal payload fraction μ_{net} between the two methods ranges from 0.6 to 1.3%.

Sensitivity Analysis

A first-order approximation of the change in maximum payload produced by changes in the technology assumptions can be performed through a sensitivity analysis. The net mass fraction μ_{net} is computed by dividing Eq. (1) by m_0 and substituting the definitions for m_{tank} and m_{pp}:

$$\mu_{\text{net}} = 1 - (1 + K_t)\frac{m_{\text{prop}}}{m_0} - \frac{\alpha P}{m_0} \tag{16}$$

Expanding Eq. (16) in a Taylor series about the nominal technology parameters α^* and K_t^* and keeping only the first-order terms results in

$$\delta\mu_{\text{net}} = \left.\frac{\partial \mu_{\text{net}}}{\partial \alpha}\right|_* \delta\alpha + \left.\frac{\partial \mu_{\text{net}}}{\partial K_t}\right|_* \delta K_t \tag{17}$$

where $\delta\mu_{\text{net}} = \mu_{\text{net}} - \mu_{\text{net}}^*$ is the perturbation from the optimal solution and $\delta\alpha$ and δK_t are defined as the respective perturbations from the nominal values. By taking the respective partial derivatives of μ_{net} as defined by Eq. (16), the first-order approximation becomes

$$\delta\mu_{\text{net}} = -\left.\frac{P}{m_0}\right|_* \delta\alpha - \left.\frac{m_{\text{prop}}}{m_0}\right|_* \delta K_t \tag{18}$$

The sensitivity coefficients $\partial\mu_{\text{net}}/\partial\alpha$ and $\partial\mu_{\text{net}}/\partial K_t$ are simply minus the optimal power and optimal propellant mass divided by m_0, respectively.

The sensitivity-coefficient curves for the specific mass $\partial\mu_{\text{net}}/\partial\alpha$ for all three cases are presented in Fig. 4. The payload sensitivity to changes in α decreases as the trip time increases. The range of $\partial\mu_{\text{net}}/\partial\alpha$ for the two realistic vehicles (cases 2 and 3) is from -0.033 to -0.005 kW/kg. As an example, if the specific mass is doubled from $\alpha = 25$ to $\alpha = 50$ kg/kW and $\partial\mu_{\text{net}}/\partial\alpha = -0.015$ kW/kg for the corresponding trip time, the net mass fraction will be reduced by approximately 0.375. The sensitivity-coefficient curves for the tankage fraction $\partial\mu_{\text{net}}/\partial K_t$ are presented in Fig. 5, and these curves also exhibit a decrease in payload sensitivity as the trip time increases. As a second example, if the tankage fraction is doubled from $K_t = 0.15$ to 0.3 and $\partial\mu_{\text{net}}/\partial K_t = -0.2$ for the corresponding trip time, the net mass fraction will be reduced by approximately 0.03. Therefore, the optimal payload is much more sensitive to uncertainties in α than to uncertainties in K_t.

First-order changes in payload performance because of technology uncertainties can be estimated by Eq. (18), and therefore the need to re-solve the vehicle–trajectory optimization problem for different values of α and K_t is eliminated. Several first-order estimates of payload deviations for both the NEP and SEP spacecraft have been calculated, and the results are summarized in Table 3. The linearized μ_{net} is computed by using Eq. (18) and the corresponding optimal solution from the previous section. Both α and K_t are simultaneously perturbed by ±40% from their nominal values, as indicated by Table 3. The corresponding optimal net mass fractions are obtained for the perturbed α and K_t values by re-solving the

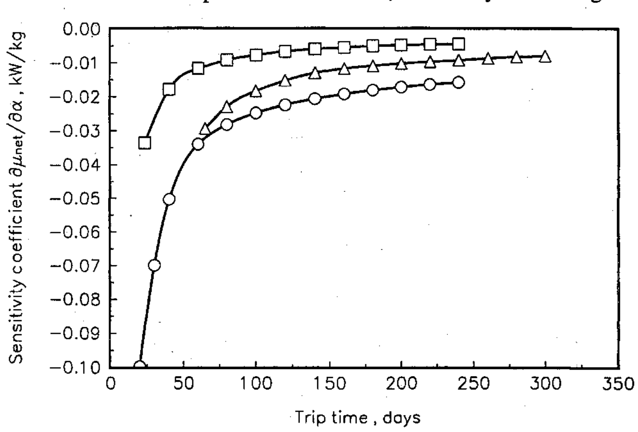

Fig. 4 Net-mass-fraction sensitivity for α vs trip time: ○, case 1; △, case 2; and □, case 3.

Table 3 Comparison between linearized and optimal solutions

Propulsion mode	t_f, days	α, kW	K_t	μ_{net} (linearized)	μ_{net} (optimal)	μ_{net} error, %
NEP	120	35	0.21	0.182	0.182	−0.02
		15	0.09	0.515	0.518	−0.54
	260	35	0.21	0.478	0.482	−0.87
		15	0.09	0.672	0.680	−1.16
SEP	60	35	0.14	0.435	0.437	−0.46
		15	0.06	0.679	0.684	−0.73
	240	35	0.14	0.750	0.752	−0.27
		15	0.06	0.844	0.848	−0.47

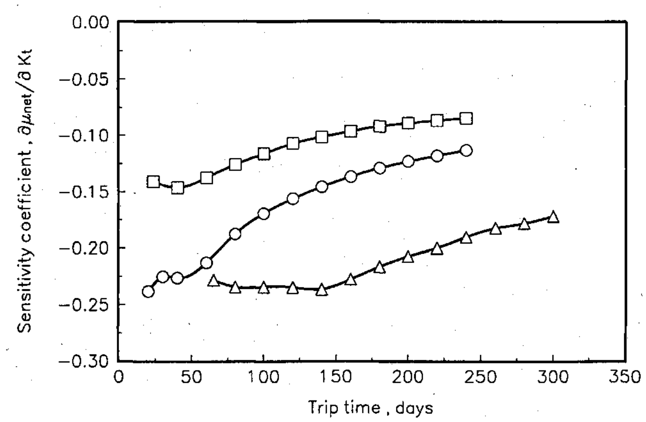

Fig. 5 Net-mass-fraction sensitivity for K_t vs trip time: ○, case 1; △, case 2; and □, case 3.

maximum-payload problem with SQP, and the solutions are presented in Table 3. It is observed that the error between the true optimal solution and the linearized estimate of μ_{net} ranges from 0.02 to 1.16%.

Conclusions

A quick and efficient method for obtaining optimal vehicle–trajectory combinations for lunar missions using EP has been developed. The vehicle–trajectory optimization involves maximizing the payload for a one-way, fixed-trip-time, planar transfer from circular Earth orbit to circular low lunar orbit with a thrust–coast–thrust engine sequence. The spacecraft design variables are the input power P and specific impulse I_{sp}, and the trajectory shaping parameters are the powered escape and capture times, translunar coast time, and initial Earth–moon geometry. The robustness and efficiency of the solution method for this complex coupled optimization problem is improved by replacing the long-duration escape and capture spiral trajectories with curve fits of universal low-thrust trajectory solutions.

Several maximum-payload solutions have been obtained for a wide range of trip times for both NEP and SEP spacecraft. The optimal NEP vehicle–trajectory solutions demonstrate excellent agreement with published results that utilize detailed trajectory simulation and optimal-control techniques. A sensitivity analysis of the assumed technology level has been performed, and the linearized results show an excellent match with the corresponding true optimal solutions.

Although only ion thrusters have been considered, this approach could easily be extended to include arcjet and magnetoplasmadynamic thrusters. The vehicle–trajectory optimization method presented here for EP lunar missions is important as a design tool for a spacecraft and mission designers.

References

[1]Gilland, J. H., "Mission and System Optimization of Nuclear Electric Propulsion Vehicles for Lunar and Mars Missions," NASA CR-189058, Dec. 1991.

[2]Palaszewski, B., "Electric Propulsion for Lunar Exploration and Lunar Base Development," AIAA Paper LBS-88-005, April 1988.

[3]Kluever, C. A., and Pierson, B. L., "Vehicle-and-Trajectory Optimization of Nuclear Electric Spacecraft for Lunar Missions," *Journal of Spacecraft and Rockets*, Vol. 32, No. 1, 1995, pp. 126–132.

[4]Hack, K. J., George, J. A., and Dudzinski, L. A., "Nuclear Electric Propulsion Mission Performance for Fast Piloted Mars Missions," AIAA Paper 91-3488, Sept. 1991.

[5]Hack, K. J., George, J. A., Riehl, J. P., and Gilland, J. H., "Evolutionary Use of Nuclear Electric Propulsion," AIAA Paper 90-3821, Sept. 1990.

[6]Oleson, S. R., "An Analytical Optimization of Electric Propulsion Orbit Transfer Vehicles," NASA CR-191129, May 1993.

[7]Oleson, S. R., "Influence of Power System Technology on Electric Propulsion Missions," AIAA Paper 94-4138, Aug. 1994.

[8]Perkins, F. M., "Flight Mechanics of Low-Thrust Spacecraft," *Journal of the Aerospace Sciences*, Vol. 26, No. 5, 1959, pp. 291–297.

[9]Szebehely, V. G., *Theory of Orbits, the Restricted Problem of Three Bodies*, 1st ed., Academic, New York, 1967, pp. 7–21.

[10]Kluever, C. A., and Chang, K.-R., "Near-Optimal Low-Thrust Lunar Trajectories," *Journal of Guidance, Control, and Dynamics* (to be published).

[11]Pierson, B. L., "Sequential Quadratic Programming and its use in Optimal Control Model Comparisons," *Optimal Control Theory and Economic Analysis*, 3rd ed., North-Holland, Amsterdam, 1988, pp. 175–193.

[12]Pouliot, M. R., "CONOPT2: A Rapidly Convergent Constrained Trajectory Optimization Program for TRAJEX," General Dynamics, Convair Division, GDC-SP-82-008, San Diego, CA, Jan. 1982.

F. H. Lutze
Associate Editor